Relation Between Oceanic Plate Structure, Patterns of Interplate Locking and Microseismicity in the 1922 Atacama Seismic Gap

Diego González-Vidal[1] , Marcos Moreno[2] , Christian Sippl[3] , Juan Carlos Baez[4] , Francisco Ortega-Culaciati[5] , Dietrich Lange[6] , Frederik Tilmann[7,8] , Anne Socquet[9], Jan Bolte[10] , Joaquin Hormazabal[5], Mickael Langlais[9] , Catalina Morales-Yáñez[11] , Daniel Melnick[1] , Roberto Benavente[11,12], Jannes Münchmeyer[9], Rodolfo Araya[13], and Benjamin Heit[7]

[1]Departamento de Geofísica, Facultad de Ciencias Físicas y Matemáticas, Universidad de Concepción, Concepción, Chile, [2]Department of Engineering and Geotectonic, Pontifical Catholic University of Chile, Santiago, Chile, [3]Institute of Geophysics, Czech Academy of Sciences, Prague, Czech Republic, [4]National Seismological Center, Faculty of Physical and Mathematical Sciences, University of Chile, Santiago, Chile, [5]Department of Geophysics, Faculty of Physical and Mathematical Sciences, University of Chile, Santiago, Chile, [6]GEOMAR Helmholtz Centre for Ocean Research Kiel, Kiel, Germany, [7]Department of Geophysics, Deutsches GeoForschungsZentrum GFZ, Wissenschaftpark "Albert Einstein", Potsdam, Germany, [8]Institute of Geological Sciences, Freie Universität Berlin, Berlin, Germany, [9]University Grenoble Alpes, University Savoie Mont Blanc, CNRS, IRD, University Gustave Eiffel, ISTerre, Grenoble, France, [10]Department of Mathematics, University of Kiel, Kiel, Germany, [11]Department of Civil Engineering, Universidad Católica de la Santísima Concepción, Concepción, Chile, [12]National Research Center for Integrated Natural Disaster Management (CIGIDEN), Santiago, Chile, [13]Departamento de Ingeniería Matemática & CI2MA, Universidad de Concepción, Concepción, Chile

Abstract We deployed a dense geodetic and seismological network in the Atacama seismic gap in Chile. We derive a microseismicity catalog of >30,000 events, time series from 70 GNSS stations, and utilize a transdimensional Bayesian inversion to estimate interplate locking. We identify two highly locked regions of different sizes whose geometries appear to control seismicity patterns. Interface seismicity concentrates beneath the coastline, just downdip of the highest locking. A region with lower locking (27.5°S–27.7°S) coincides with higher seismicity levels, a high number of repeating earthquakes and events extending toward the trench. This area is situated where the Copiapó Ridge is subducted and has shown previous indications of both seismic and aseismic slip, including an earthquake sequence in 2020. While these findings suggest that the structure of the downgoing oceanic plate prescribes patterns of interplate locking and seismicity, we note that the Taltal Ridge further north lacks a similar signature.

Plain Language Summary Deformation along plate boundaries can occur seismically (i.e. through earthquakes) as well as aseismically (i.e. slipping slowly), and it is important to understand where each of these modes is dominant. Along the Chilean subduction contact, North-Central Chile is the only place where aseismic deformation episodes have been observed so far. In order to study these processes in detail, we deployed and operated dense geodetic and seismological networks in this region. Analyzing the data collected by these networks, we find notable relationships between seismic and aseismic processes. Thousands of small earthquakes are found at the boundaries of locked regions, whereas no small earthquakes are found at their interior. Thus, implying such regions are mechanically coupled, that is, currently accumulating elastic deformation energy that will 1 day be released during a large earthquake. Along the North-Central Chilean plate boundary, there is one region (around 27.5°S) that shows many signs of aseismic deformation. It is located where a chain of seamounts is being subducted, which is likely responsible for the different behavior of this segment.

1. Introduction

Relative motion along the subduction zone plate interface is partitioned between seismic and aseismic processes (e.g., Perfettini et al., 2010). The seismogenic zone of the megathrust accumulates slip deficit and releases it seismically during large earthquakes (Lay et al., 2012). In contrast, the adjacent updip and downdip regions tend to exhibit aseismic slip that accounts for part or the totality of the plate convergence (e.g., Peng & Gomberg, 2010).

Methodology: Diego González-Vidal, Christian Sippl, Francisco Ortega-Culaciati, Dietrich Lange, Roberto Benavente, Rodolfo Araya
Resources: Joaquin Hormazabal, Roberto Benavente, Rodolfo Araya, Benjamin Heit
Software: Marcos Moreno, Christian Sippl, Juan Carlos Baez, Francisco Ortega-Culaciati, Dietrich Lange, Jan Bolte, Jannes Münchmeyer
Visualization: Diego González-Vidal, Marcos Moreno, Christian Sippl
Writing – original draft: Diego González-Vidal, Marcos Moreno, Christian Sippl, Juan Carlos Baez
Writing – review & editing: Diego González-Vidal, Marcos Moreno, Christian Sippl, Juan Carlos Baez, Francisco Ortega-Culaciati, Dietrich Lange, Frederik Tilmann, Anne Socquet, Jan Bolte, Joaquin Hormazabal, Mickael Langlais, Catalina Morales-Yáñez, Daniel Melnick, Roberto Benavente, Jannes Münchmeyer, Rodolfo Araya, Benjamin Heit

The amount of convergence accommodated in large earthquakes versus continuous or transient creep is highly variable along strike in many subduction zones (Métois et al., 2016). Different forms of aseismic slip are observed along the plate interface. Slow-slip events (SSEs) are days-to-months long aseismic slip pulses that usually occur at the downdip end of the plate interface and are often accompanied by non-volcanic tremor (Schwartz & Rokosky, 2007). However, SSEs have also been observed in the shallowest part of the plate interface (e.g., Araki et al., 2017) or within the seismogenic zone (e.g., Obara & Kato, 2016; Ohta et al., 2006). Aseismic slip transients have also been observed to precede large earthquakes (e.g., Ito et al., 2013; Radiguet et al., 2016; Socquet et al., 2017; Voss et al., 2018), as a mixture of slow deformation and foreshocks (Bedford et al., 2015). Finally, aseismic slip unrelated to large earthquakes has also been observed along weakly locked segments of the plate interface (Okamoto et al., 2022). Increased seismicity rates or swarm-like sequences have been found to occur in direct vicinity to—and likely triggered by—aseismic transients (Hirose et al., 2014; Vallée et al., 2013). Repeating earthquakes, recurring small events that repeatedly rupture the same fault area, are thought to be a direct consequence of ongoing aseismic deformation in their surroundings (Igarashi et al., 2003; Uchida & Bürgmann, 2019).

SSEs along the Chilean margin appear to be rare or at least more subtle. North-Central Chile is one of the few sites where transient slow-slip events have been observed independently from large megathrust earthquakes in Chile. A SSE event of ∼18 months duration with a maximum slip of about 50 cm was observed at the deepest part of the plate interface in 2014 and 2015 (Klein, Duputel, et al., 2018), and again in 2020 (Klein et al., 2023). Swarm-like seismicity sequences have been observed in 2006 and 2015 close to the town of Caldera, updip of the SSE's location (Holtkamp et al., 2011; Ojeda et al., 2023), as well as ∼50–100 km further south in 2020 (Klein et al., 2021). However, this segment of the margin has until recently only been sparsely instrumented, so that a first more comprehensive analysis of its seismicity has only recently been undertaken (Pastén-Araya et al., 2022). The Atacama region was struck by a great ($M_w \sim 8.5$) earthquake in 1922 and by a similar event in 1819 (Figure 1a), thus being considered a mature seismic gap, at risk of breaking in a great subduction earthquake (e.g., Yáñez-Cuadra et al., 2022). In September 2020, an earthquake sequence occurred at 28°S. It consisted of a magnitude M_w6.9 mainshock and a M_w6.4 aftershock, lasting several weeks and involving numerous low magnitudes events (Klein et al., 2021).

In this study, we deployed a dense network of 85 seismic stations complementing 16 stations already installed in the region (see Figures S1, S6, and Text S3, in Supporting Information S1). Additionally, we deployed 28 continuous GNSS stations to densify the already existing network composed by 42 GNSS sites (see Figures S1–S3, Text S1 in Supporting Information S1). We created a high-resolution microseismicity catalog comprising more than 30,000 events occurring for 15 months since November 2020. We compare this seismicity to the interplate locking, which is constrained by GNSS secular rates and estimated using a transdimensional Bayesian approach. In this scheme, the spatial resolution of the locking model is obtained in a data-driven manner without the need for a priori smoothing. From these observations, we derive constraints on the interplay between seismic and aseismic processes in the region. In the following sections, we first describe the derivation of the locking model from geodetic observations, as well as the seismicity catalog from the measured seismic waveforms.

2. A Transdimentional Bayesian Estimation of Interplate Locking

We used data from a total of 70 GNSS stations situated between 23°S and 32°S. This data set includes 28 newly deployed stations, which were added to the existing backbone network of the National Seismological Center of Chile (Figure 1, Table S1 in Supporting Information S1). We processed the GNSS data using Bernese software to produce daily positional time series for the period between January 2018 and February 2023 (Dach et al., 2015; Teunissen & Montenbruck, 2017; VMF Data Server, 2021). Then, we clean the time series and adjust a trajectory model to isolate the secular velocity for each station in the ITRF2014 system (Báez et al., 2018; Bevis & Brown, 2014; Huang et al., 2012; Köhne et al., 2023). We refer the reader to Text S1 in Supporting Information S1 for further details.

Over the analyzed period, no recurrent transient motions are observed in the GNSS time series or in the residuals of the trajectory model. The estimated horizontal velocities show a gradual increase north of 29°S (Figure 1b). Between 29°S and 31°S, a decrease in the magnitude of the velocities is observed in the area of the 2015 (M_w8.3) Illapel earthquake rupture (Figure 1a). Vertical motion shows subsidence at coastal stations at 27.2°S and 29°S, which may be related to changes in the depth of the locked zone.
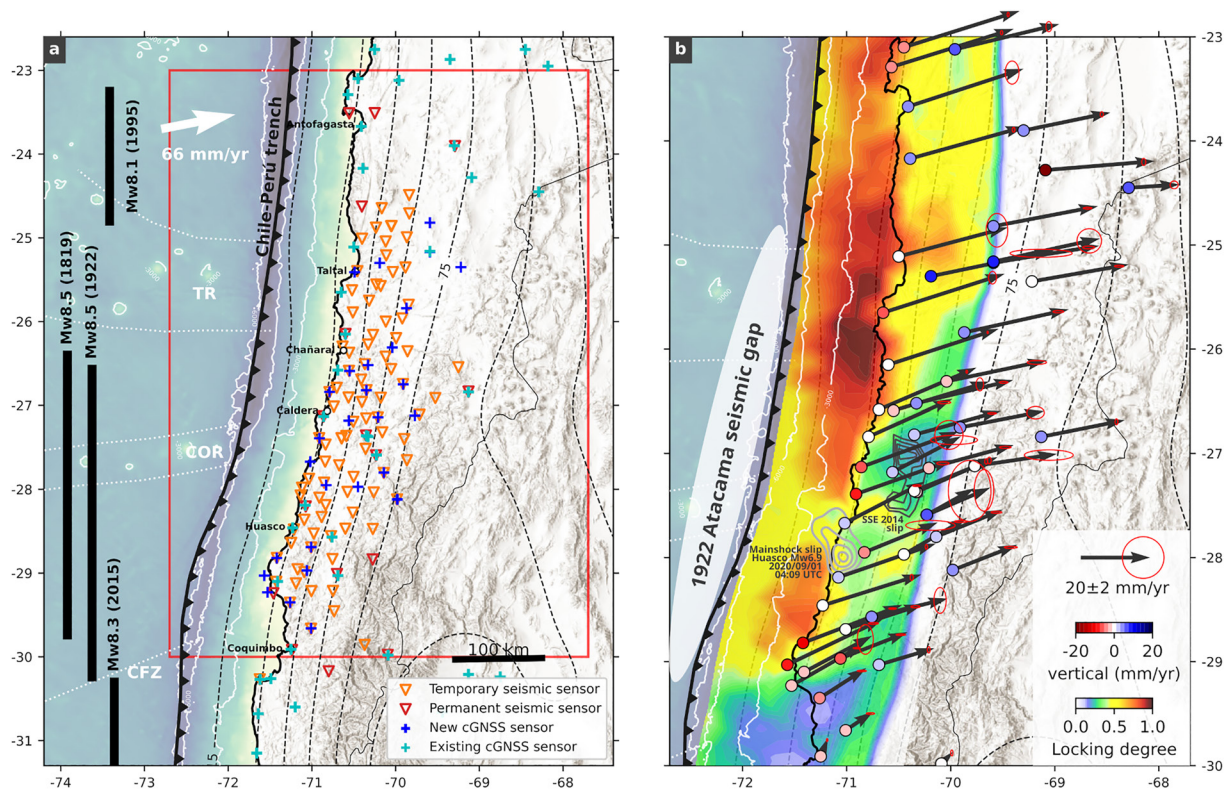
Figure 1. (a) Map view showing the distribution of existing and new GNSS and seismic networks in North-central Chile. The slab surface after model slab2 (Hayes et al., 2018) is shown with dashed black contour lines at 15 km intervals, the black barbed line marks the Chile-Perú trench and the white dotted outlines show prominent seafloor features (CFZ—Challenger Fracture Zone; COR—Copiapó Ridge; TR—Taltal Ridge). Rupture extents of historical megathrust earthquakes ($M_w > 8$) are shown on the left. The red rectangle shows the extent of subfigure (b). (b) Horizontal (vectors) and vertical (point coloring) velocities and uncertainties (red ellipses) of GNSS stations used in this study, shown together with the derived mean interplate locking model. The extent of the 1922 Atacama seismic gap is shown by the white ellipse on the left (modified from Molina et al. (2021)). Black contours mark the location of aseismic slip during the 2014 SSE (Klein, Duputel, et al., 2018) (every 50 mm starting at 200 mm), while gray contours mark the mainshock slip of the M_w 6.9 Atacama sequence event on 01 September 2020 04:09 UTC (Klein et al., 2021) (every 20 mm starting at 60 mm).

We utilize the resulting velocities to estimate the degree of locking along the subduction megathrust for the period from 2018 to the end of 2022. To compute Green's functions, we employ the backslip model (Aagaard et al., 2013; Savage, 1983), and incorporate the interseismic viscoelastic relaxation using a finite element model. This approach incorporates the same methodology and rheological properties as utilized by Li et al. (2015). The interseismic deformation field in the forearc of northern and central Chile is affected not only by contraction induced by plate coupling, but also by continental deformation driven by the partitioning of tectonic deformation along continental structures (e.g., Yáñez-Cuadra et al., 2022). Therefore, to estimate the degree of locking, it is necessary to account for the contribution of continental deformation in the regional displacement field. To achieve this, we subtract the velocity field predicted by the deformation tensor proposed by Yáñez-Cuadra et al. (2022) from the estimated GNSS displacements (Figure 1b). These corrected velocities are then utilized in the locking inversion, enabling a more reliable assessment of the locking degree.

We estimate the degree of locking through a Bayesian transdimensional inversion method (Bodin & Sambridge, 2009; Green, 1995; Sambridge, 2013), employing the reversible jump Markov chain Monte Carlo (rj-MCMC) technique to obtain samples from the posterior probability function of backslip. This approach allows for a comprehensive analysis of the locking degree by incorporating the variability and uncertainty inherent in the estimation process. In our approach, the spatial distribution of locking is discretized by Voronoi cells (Dettmer et al., 2014). The number and location of Voronoi cell centers are not fixed, but are allowed to vary according to a stochastic process. We truncate the solutions to ensure positive values of backslip, consistent with the physical model of strain accumulation due to locking at the subduction megathrust. Additionally, we impose restrictions on the backslip values to prevent them from exceeding the plate convergence rate, ensuring physical plausibility

(backslip ≥0 and ≤convergence rate between the tectonic plates). We note that this methodology follows Bayesian parsimony, where the size of the Voronoi cells slip discretization is driven by the resolving capability of the data and the properties of the physical model. Therefore, in contrast to typical least-squares optimization approaches that need some prior spatial smoothing constraint to solve the inherently ill-posed slip inversion (e.g., Ortega-Culaciati et al., 2021), our approach does not require such a subjective smoothing of the slip distribution (see Text S2 in Supporting Information S1).

Using the transdimensional approach, we generate an ensemble of more than 1 million locking models, from which we compute the mean locking distribution shown in Figure 1b. The model fits well the horizontal and vertical observations (Figure S4 and S5 in Supporting Information S1) and exhibits a pattern of increasing locking degree toward the north, consistent with the gradient observed in the surface displacement field. Our results show high values of interplate locking in the offshore region, with mostly lower values (<0.6) beneath the onshore regions. The margin north of 27.5°S appears to be highly locked, with the highest values around 26°S. A second, smaller highly locked area is located in the southern part of the study area, around 28–29°S. It is separated from the northern locking high by a narrow region centered around 27.7°S, which exhibits a significantly lower degree of locking. No values exceeding 0.5 are observed in this region. Locking degree is low in the southernmost part of the study region, possibly due to the effect of the postseismic signals from the 2015 (M_w8.3) Illapel earthquake.

3. Seismicity Catalog

We analyzed data from 101 seismic stations located in the Atacama seismic gap (24.4°S–30.3°S) that continuously recorded waveforms from November 2020 to July 2022 (Figure 1). Given the large amount of data, we used an automated earthquake detection and location workflow based on machine learning techniques for phase picking (EQTransformer; Mousavi et al., 2019, 2020; Münchmeyer et al., 2022; Woollam et al., 2022) and phase association (GaMMA; Zhu et al., 2022). We define events as having at least 7 P- and 4 S-phases resulting in a seismicity catalog that features 30,560 events, comprising 469,980 P-phases and 391,350 S-phases. We then successively relocated this catalog based on a 1D as well as a 2D velocity model (Figure S9 in Supporting Information S1) that was derived from a subset of our data (Havskov et al., 2020; Kissling et al., 1994; Thurber & Eberhart-Phillips, 1999), before eventually applying hypoDD (Waldhauser & Ellsworth, 2000) to obtain double-difference relocations (see Figure S7 and Text S3 in Supporting Information S1). We estimate average location errors to be <5 km inside the network, while they increase to 10–25 km outside the network toward the trench and volcanic arc (Figure S8 in Supporting Information S1). Local magnitudes range from 0.6 to 5.7 and we obtain an overall completeness magnitude of 1.6 (Figure S10 in Supporting Information S1).

The seismicity catalog is presented in Figure 2. The apparent decay of seismicity north of ~24.5°S and south of ~29.5°S is likely due to the lower detection capability plus shorter deployment times in such regions. A continuous band of high background seismicity beneath the coastline is the most prominent feature of the catalog. Events in this band, located ~30–100 km from the trench, define two parallel planes with <10 km vertical separation in profile view (Figures 2b–2e). While the upper plane likely corresponds to the deeper portion of the plate interface, its deepest (~75 km) portion is located inside the downgoing slab and corresponds to the upper band of an occasionally visible double seismic zone (DSZ, e.g., Brudzinski et al., 2007; Sippl et al., 2018). Seismicity is scarce at the shallower part of the plate interface, extending closer to the trench along a total of four or five narrow features (Figure 2a), that also host significant concentrations of repeating earthquakes (see Text S4 in Supporting Information S1). Seawards of the trench, scattered events south of 26°S likely occurred in the outer rise region. Due to their location far outside the network, the depth of these events is very badly defined. East of the coastline, seismicity is largely found inside the downgoing slab, confined to the uppermost 25–30 km of the lithosphere. Most of this intraslab seismicity occurs at ~50–120 km depth, between ~150 and 300 km distance from the trench. The geometry and vigor of intraslab seismicity is highly variable along strike. In the north (Figure 2b), most seismicity occurs in the uppermost 10–15 km of the slab, whereas deeper levels (20–30 km below slab surface) are most active further south (Figures 2d and 2e). In profiles c and d of Figure 2, a clear DSZ with about 15 km separation between both bands is visible. The southward transition to the Pampean flat slab is accompanied by high seismicity levels deeper within the downgoing slab. We obtain 3,431 upper plate seismic events, defined as those located at <15 km depth and >5 km above the top of the subducted slab. Their occurrence rate is significantly increased during local daytime, suggesting a predominance of mining blast activity (Figure S11 in Supporting Information S1).
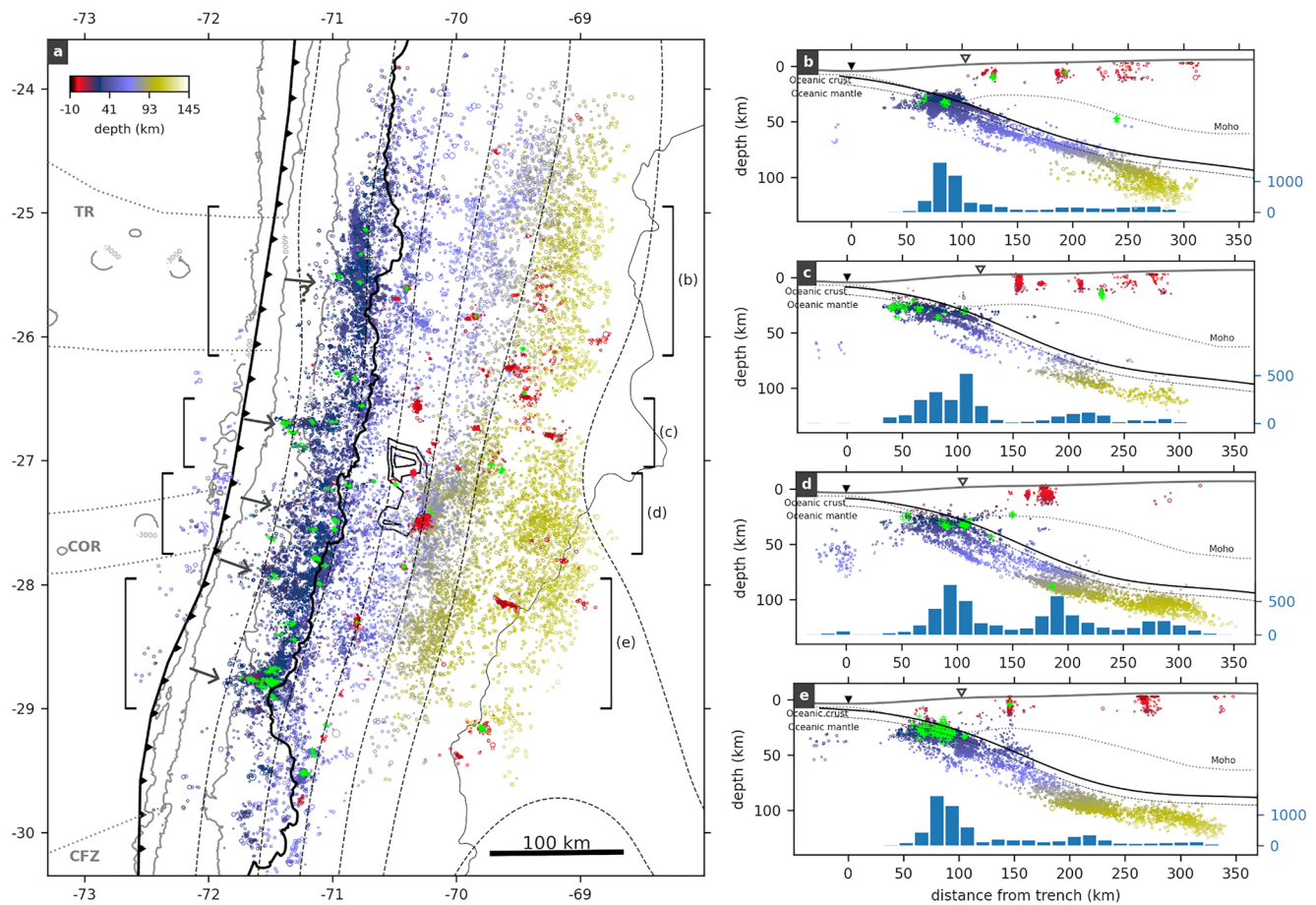
Figure 2. Map view (a) and profile projections (b–e) of the 30,560 hypocenters in the seismicity catalog, color-coded by depth. Families of repeaters are shown by green plus markers. The locations and swath widths of the profile projections are indicated by the black brackets in subfigure (a). The black barbed line in the map view plot marks the location of the trench and the dotted pale gray lines show prominent seafloor features. The slab2 slab surface (Hayes et al., 2018) is shown with dashed contour lines in (a) and with solid lines in the profile plots. The dashed black line in the profiles shows the inferred oceanic Moho located 7 km below the slab2 surface. The dotted thin line shows the continental Moho from Tassara and Echaurren (2012). The position of the trench is marked by black inverted triangles and the coastline is marked by white inverted triangles. The blue histograms show earthquake numbers along the profiles, excluding upper plate seismicity. The gray arrows in the map show narrow features of seismicity extending toward the trench.

4. Discussion

4.1. Relation Between Microseismicity and Interplate Locking

Figure 3 summarizes the spatial relationship between interplate locking and the occurrence of microseismicity along the North-Central Chile margin. The highest concentration of microseismicity is found to occur just seawards and beneath the coastline (Figure 3a), with hypocentral depths between ~25 and 40 km. This location roughly corresponds to the landward edge of the highly locked regions, indicating that most seismicity occurs where locking starts to decrease in the downdip direction (Figure 3c). In contrast, the shallower part of the megathrust (depths <30 km) exhibits a significant absence of seismicity. The little seismicity that occurs there extends as northwest lineaments toward the trench, primarily in regions characterized by low coupling (Figure 2). When projected in the along-strike direction (Figure 3b), the highest seismicity concentrations and the largest number of repeating earthquakes (Uchida & Matsuzawa, 2013) can be found along the northern and southern terminations of the southern highly locked patch.

A very similar pattern of seismicity and interplate locking was found south of the study region (Sippl et al., 2021), where it was interpreted as the signature of mechanically coupled asperities on the megathrust. Accumulation of convergence over most of the seismic cycle creates a "halo" of high stresses around the downdip edge of highly locked regions (e.g., Moreno et al., 2018; Schurr et al., 2020). This "halo" may be the cause of the high levels of
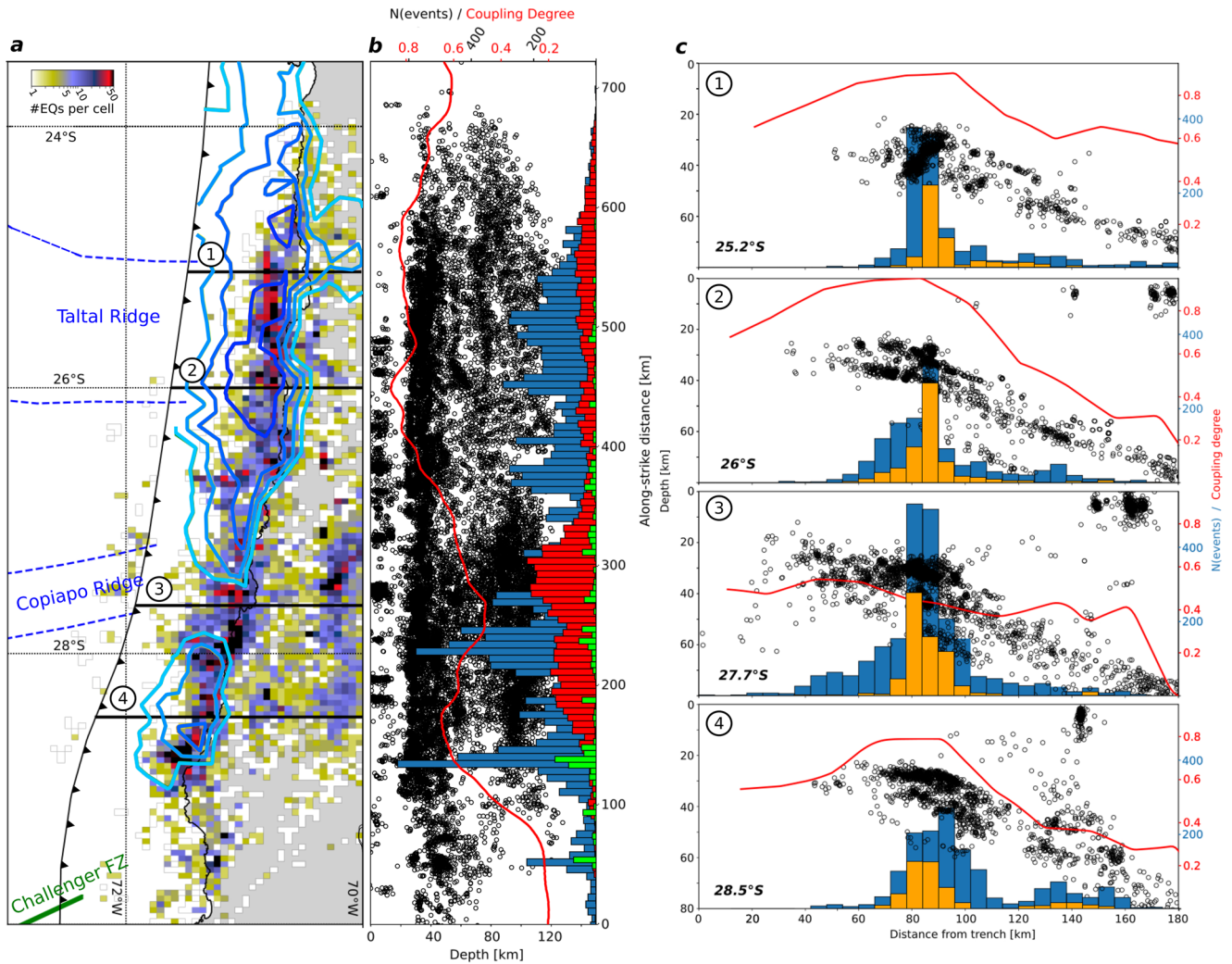
Figure 3. Correlating seismicity and interplate locking patterns. (a) Map view plot of seismicity density, showing contours of mean interplate locking (0.6, 0.7, 0.8, and 0.9) as well as features on the downgoing oceanic plate. Black lines mark the locations of the W-E profiles shown in subfigure (c). (b) Projection of seismicity onto a single longitudinal plane. Histogram in blue represents the amount of seismicity in the vicinity of the plate interface (20–70 km depth), histogram in red the intermediate-depth seismicity (depth >70 km), and histogram in green the repeating earthquakes. Red line shows the average locking degree of the uppermost 40 km of the plate interface according to the locking model shown in Figure 1b. (c) Narrow W-E profiles of seismicity (swath width ±0.2° around nominal latitude), showing event numbers in the depth range 20–70 km with the blue histograms. Orange histograms show numbers of earthquakes within 5 km vertical distance from the plate interface after model slab2. Red line represents the average locking degree in a swath of ±0.1° around the profile location.

background seismicity we observe on the deeper part of the plate interface, and lack of seismicity in locked zones. The weak locking and high seismicity we obtain around 27.7°S likely represents a segment of the megathrust that features more aseismic deformation. Low locking in this location is a stable feature across all published locking maps of the area (Klein, Métois, et al., 2018; Métois et al., 2016; Yáñez-Cuadra et al., 2022), and indicators for slow slip processes have been observed here (Section 4.2; Figure 4). The seismicity in the shallower part of the plate interface in this region is probably driven by such slow slip processes, which explains its absence in other, more highly locked regions of the megathrust.

The southern termination of the southern locked patch around 29°S features increased seismicity levels and elevated numbers of repeating earthquakes (Figure 2), similar to the region around 27.7°S. While the resolution of our catalog is very low south of ~29°S, Sippl et al. (2021) show an extended zone of increased shallow plate interface seismicity up to ~30.5°S. This could hint at the presence of aseismic processes related to the incoming Challenger Fracture Zone (Figures 1a and 3), which is thought to have prescribed the northern termination of the 2015 M_w 8.3 Illapel earthquake (e.g., Poli et al., 2017; Tilmann et al., 2016).
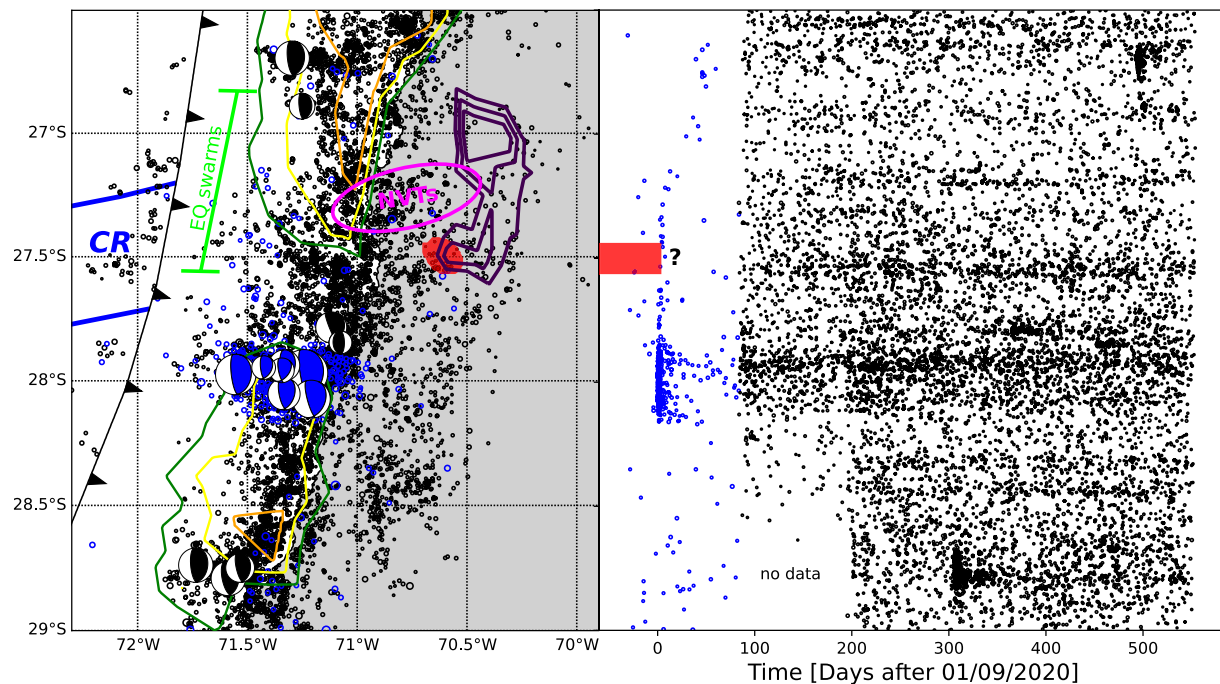
Figure 4. (left) Zoom-in to the weakly locked region (∼27.5°S) onshore of the incoming Copiapó Ridge. Blue circles mark earthquakes between 01 August and 23 November 2020, taken from the CSN catalog (Barrientos, 2018) and mostly showing the 2020 Atacama sequence (Klein et al., 2021). Black circles show earthquakes from our catalog, starting on 23 November 2020. Beachballs show lower-hemisphere projections of focal mechanisms for events with magnitude ≥4.8, taken from GEOFON. Purple contours mark the location of aseismic slip during the 2014 SSE (Klein, Duputel, et al., 2018), the red dot marks the approximate position of the 2020 SSE (Klein et al., 2023). The latitudinal range of earthquake swarms in 1973, 1979, 2006, and 2015 (Ojeda et al., 2023) is indicated by the green bracket, and the pink ellipse shows where non-volcanic tremor was identified in 2019 (Pastén-Araya et al., 2022). Green, yellow and orange lines mark locking degree contour lines of 0.6, 0.7, and 0.8. (right) Plot of earthquake latitudes against time, showing CSN catalog earthquakes in blue and our catalog in black. A horizontal stripe of increased seismicity is present at the latitude of the 2020 Atacama sequence. The red stripe marks the 2020 SSE.

4.2. Seismic and Aseismic Signature of the Copiapó Ridge

Figure 4 summarizes observations of seismic and aseismic processes in the vicinity of the incoming Copiapó Ridge. A prominent offshore seismic swarm occurred in the region in 2006 (Holtkamp et al., 2011), and similar swarm occurrences have been reported for the years 1973, 1979, and 2015 (e.g., Ojeda et al., 2023). The 2014 SSE was situated further downdip but covered the same latitudinal range (Klein, Duputel, et al., 2018). A similar SSE was identified starting in March 2020, confined to the southern part of the 2014 SSE (Klein et al., 2023). Aseismic slip continued at least until September 2020, when the Atacama seismic sequence (see below) began to shadow the SSE signal. Non-volcanic tremor events observed in 2019 (Pastén-Araya et al., 2022) occurred directly updip of the 2014 SSE. In September 2020, only 2.5 months before the start of our catalog and GNSS observations, the Atacama seismic sequence occurred, featuring three major earthquakes of $M_w > 6$. In addition, unusually large amounts of aseismic slip, equivalent to M_w 6.8, occurred within the weakly coupled patch between the mainshock of the Atacama seismic sequence and the southern edge of the 2014 SSE (Klein et al., 2021). This sequence was situated along the southern edge of our inferences of weak locking, whereas all previously mentioned observations of earthquake swarms, SSEs and NVTs were situated 50–100 km further north (Figure 4). We found continued elevated background seismicity rates throughout the studied time interval in the latitudinal range of the 2020 Atacama sequence, accompanied by some repeating earthquakes (Figure 2).

Taken together, all these observations highlight the complex interplay of seismic and aseismic processes in the direct vicinity of the subduction of the Copiapó Ridge. It has previously been shown that elevated roughness on the downgoing plate leads to reduced interplate coupling (Wang & Bilek, 2014), as well as the formation of weakly coupled, creeping segments that may act as "barriers" to large earthquakes due to the lack of stress accumulation. Subducting ridges have also been shown to feature enhanced hydration of the downgoing plate, which can further reduce interplate coupling through the release of fluids and the subsequent increase of pore fluid pressure on the plate interface (e.g., Moreno et al., 2014). While these observations suggest that the region

around 27.7°S represents a weakly locked "barrier" that may hinder the propagation of large megathrust earthquakes, the two last major earthquakes in 1922 and 1819 likely ruptured across this region (Figure 1a). North of 26°S, the Taltal Ridge impinges onto the North Chilean margin. Although its offshore bathymetric expression is similar to the Copiapó Ridge (Figure 1), we do not retrieve a region of lower interplate locking degree or elevated seismicity in this region (Figures 1 and 3). Whether this implies that the Taltal Ridge has only recently started to be subducted, or whether it possesses properties that clearly distinguish it from the Copiapó Ridge, is currently unclear. Another possible explanation is that the barrier effect of a ridge could be temporary and induced by seismic sequences, as observed at the Copiapó Ridge. In contrast, although the Taltal Ridge did not exhibit significant seismic activity during the observation period, it remains uncertain if this pattern will persist in the future.

4.3. Intraslab Seismicity

Here we only provide a brief general overview of intraslab seismicity, with a more detailed analysis delegated to a future study. Our catalog shows Nazca plate intraslab seismicity occurring at depths ranging 35 to ∼120 km. A DSZ can be recognized, with its upper seismicity band most vigorously active directly beneath where most plate interface seismicity occurs (Figure 2c). The lower band of the DSZ, located ∼15 km below the upper band, within the downgoing slab, shows only weak activity at depths shallower than 80 km. At larger depths, seismicity in deeper levels of the slab intensifies. Thus, it is harder to distinguish the two bands of the DSZ, as seismicity fills the gap between the two zones, in a similar manner as independently observed in Northern Chile (e.g., Sippl et al., 2018). Most of this deeper intraslab seismicity is concentrated south of 27°S, with a clear maximum around 27.4°S. Intraslab earthquakes at intermediate depths are thought to be related to dehydration processes in the downgoing oceanic lithosphere (e.g., Hacker et al., 2003; Zhan, 2020). It is widely assumed that the loci and rate of seismicity in the slab represent the distribution of fluid release at depth. The concentration of deeper seismicity around 27.4°S may be the signature of increased hydration of the downgoing Copiapó Ridge. Streaks of increased intermediate-depth seismicity have been previously shown along the trace of downgoing ocean features along the Chilean margin (e.g., Geersen et al., 2022; Kirby et al., 1996). We could hypothesize there is a direct causal link between the different signatures of the Copiapó Ridge on the plate interface (low locking degree and seismicity) and within the slab (increased seismicity), through fluid processes, for instance. Alternatively, both behaviors may be independent consequences of ridge subduction. Discriminating between these hypotheses is beyond the scope of this contribution. We note that the signature of the Taltal Ridge further north is again less clearly visible, if present at all.

5. Conclusions

We combine novel highly resolved seismological and geodetic observations and model these using frontier techniques. Our results identify a number of distinct seismic and aseismic patterns, primarily influenced by the structure of the descending Nazca Plate and the distribution of locking. Our inferred locking distribution suggests that the Atacama seismic gap consists of two highly coupled regions of different sizes, separated by a creeping corridor with higher background seismicity. The geometry of these two "asperities" appears to control seismicity patterns. While the highly locked shallow part of the plate interface presents scarce seismicity, the downdip limit of interplate locking is marked by a band of background seismicity located beneath the coastline. Interplate locking decreases significantly around 27.5°S–27.7°S, where seismicity reaches shallower depths and numerous indicators for ongoing aseismic slip processes have been observed. The subduction of the Copiapó Ridge at this latitude creates a clear signature along the megathrust and at deeper depths inside the downgoing slab, both as a consequence of bathymetric roughness and/or increased (de)hydration.

Data Availability Statement

The seismic waveforms we used in this paper to compile the earthquake catalog was retrieved from the GEOFON data centre of the GFZ German Research Centre for Geosciences and IRIS Web, and come from the networks Y6 (Tilmann et al., 2021), XZ (Socquet et al., 2025), CX (GFZ & CNRS-INSU, 2006), C1 (Universidad de Chile, 2013), C (https://www.fdsn.org/networks/detail/C/) and IU (Albuquerque Seismological Laboratory/ USGS (ASL), 2014). XZ data are archived at the EPOS-FRANCE RESIF data center (https://seismology.resif.fr/fr/reseaux/#/XZ__2020) and will be opened at the end of the project (2026). Moment tensors used in Figure 4

were retrieved from the GEOFON program of the GFZ German Research Centre for Geosciences (https://geofon.gfz-potsdam.de/eqinfo/). The earthquake catalog, GNSS time series and locking model presented in this article are available at the GFZ Data Center https://doi.org/10.5880/fidgeo.2023.018 (González-Vidal et al., 2023). The national seismic catalog was provided by the Centro Sismológico Nacional (CSN, Chile; http://www.sismologia.cl/) (Barrientos, 2018).

References

Aagaard, B. T., Knepley, M. G., & Williams, C. A. (2013). A domain decomposition approach to implementing fault slip in finite-element models of quasi-static and dynamic crustal deformation. *Journal of Geophysical Research: Solid Earth*, *118*(6), 3059–3079. https://doi.org/10.1002/jgrb.50217

Albuquerque Seismological Laboratory/USGS (ASL). (2014). Global seismograph network (GSN—IRIS/USGS) [Dataset]. Federation of Digital Seismograph Networks. https://doi.org/10.7914/SN/IU

Araki, E., Saffer, D., Kopf, A. J., Wallace, L., Kimura, T., Machida, Y., et al. (2017). Recurring and triggered slow-slip events near the trench at the Nankai Trough subduction megathrust. *Science*, *356*(6343), 1157–1160. https://doi.org/10.1126/science.aan3120

Báez, J. C., Leyton, F., Troncoso, C., del Campo, F., Bevis, M., Vigny, C., et al. (2018). The Chilean GNSS network: Current status and progress toward early warning applications. *Seismological Research Letters*, *89*(4), 1546–1554. https://doi.org/10.1785/0220180011

Barrientos, S. (2018). The seismic network of Chile. *Seismological Research Letters*, *89*(2A), 467–474. https://doi.org/10.1785/0220160195

Bedford, J., Moreno, M., Schurr, B., Bartsch, M., & Oncken, O. (2015). Investigating the final seismic swarm before the Iquique-Pisagua 2014 Mw 8.1 by comparison of continuous GPS and seismic foreshock data. *Geophysical Research Letters*, *42*(10), 3820–3828. https://doi.org/10.1002/2015GL063953

Bevis, M., & Brown, A. (2014). Trajectory models and reference frames for crustal motion geodesy. *Journal of Geodesy*, *88*(3), 283–311. https://doi.org/10.1007/s00190-013-0685-5

Bodin, T., & Sambridge, M. (2009). Seismic tomography with the reversible jump algorithm. *Geophysical Journal International*, *178*(3), 1411–1436. https://doi.org/10.1111/j.1365-246x.2009.04226.x

Brudzinski, M. R., Thurber, C. H., Hacker, B. R., & Engdahl, E. R. (2007). Global prevalence of double Benioff zones. *Science*, *316*(5830), 1472–1474. https://doi.org/10.1126/science.1139204

Dach, R., Lutz, S., Walser, P., & Fridez, P. E. (2015). *Bernese GNSS software version 5.2*. University of Bern, Bern Open Publishing. https://doi.org/10.7892/boris.72297

Dettmer, J., Benavente, R., Cummins, P. R., & Sambridge, M. (2014). Trans-dimensional finite-fault inversion. *Geophysical Journal International*, *199*(2), 735–751. https://doi.org/10.1093/gji/ggu280

Geersen, J., Sippl, C., & Harmon, N. (2022). Impact of bending-related faulting and oceanic-plate topography on slab hydration and intermediate-depth seismicity. *Geosphere*, *18*(2), 562–584. https://doi.org/10.1130/GES02367.1

GFZCNRS-INSU. (2006). *IPOC seismic network: Integrated plate boundary observatory Chile—IPOC*. GFZ Data Services. https://doi.org/10.14470/PK615318

González-Vidal, D., Moreno, M., Sippl, C., Baez, J. C., Ortega-Culaciati, F., Lange, D., et al. (2023). *GNSS time series, interplate locking model and earthquake catalog in the 1922 Atacama seismic gap, Chile*. GFZ Data Services. https://doi.org/10.5880/fidgeo.2023.018

Green, P. J. (1995). Reversible jump Markov chain Monte Carlo computation and Bayesian model determination. *Biometrika*, *82*(4), 711–732. https://doi.org/10.1093/biomet/82.4.711

Hacker, B. R., Peacock, S. M., Abers, G. A., & Holloway, S. D. (2003). Subduction factory 2. Are intermediate-depth earthquakes in subducting slabs linked to metamorphic dehydration reactions? *Journal of Geophysical Research*, *108*(B1), 2030. https://doi.org/10.1029/2001JB001129

Havskov, J., Voss, P. H., & Ottemöller, L. (2020). Seismological observatory software: 30 Yr of SEISAN. *Seismological Research Letters*, *91*(3), 1846–1852. https://doi.org/10.1785/0220190313

Hayes, G. P., Moore, G., Portner, D. E., Hearne, M., Flamme, H., Furtney, M., & Smoczyk, G. M. (2018). Slab2, a comprehensive subduction zone geometry model. *Science*, *362*(6410), 58–61. https://doi.org/10.1126/science.aat4723

Hirose, H., Matsuzawa, T., Kimura, T., & Kimura, H. (2014). The Boso slow slip events in 2007 and 2011 as a driving process for the accompanying earthquake swarm. *Geophysical Research Letters*, *41*(8), 2778–2785. https://doi.org/10.1002/2014GL059791

Holtkamp, S. G., Pritchard, M. E., & Lohman, R. B. (2011). Earthquake swarms in South America. *Geophysical Journal International*, *187*(1), 128–146. https://doi.org/10.1111/j.1365-246x.2011.05137.x

Huang, D., Dai, W., & Luo, F. (2012). Ica spatiotemporal filtering method and its application in GPS deformation monitoring. *Applied Mechanics and Materials*, *204–208*, 2806–2812. https://doi.org/10.4028/www.scientific.net/AMM.204-208.2806

Igarashi, T., Matsuzawa, T., & Hasegawa, A. (2003). Repeating earthquakes and interplate aseismic slip in the northeastern Japan subduction zone. *Journal of Geophysical Research*, *108*(B5), 1–9. https://doi.org/10.1029/2002jb001920

Ito, Y., Hino, R., Kido, M., Fujimoto, H., Osada, Y., Inazu, D., et al. (2013). Episodic slow slip events in the Japan subduction zone before the 2011 Tohoku-oki earthquake. *Tectonophysics*, *600*, 14–26. https://doi.org/10.1016/j.tecto.2012.08.022

Kirby, S., Engdahl, E. R., & Denlinger, R. (1996). Intermediate-depth intraslab earthquakes and arc volcanism as physical expressions of crustal and uppermost mantle metamorphism in subducting slabs. *Geophysical Monograph Series*, *96*, 195–214. https://doi.org/10.1029/GM096p0195

Kissling, E., Ellsworth, W. L., Eberhart-Phillips, D., & Kradolfer, U. (1994). Initial reference models in local earthquake tomography. *Journal of Geophysical Research*, *99*(B10), 19635–19646. https://doi.org/10.1029/93jb03138

Klein, E., Duputel, Z., Zigone, D., Vigny, C., Boy, J. P., Doubre, C., & Meneses, G. (2018). Deep transient slow slip detected by survey GPS in the region of Atacama, Chile. *Geophysical Research Letters*, *45*(22), 12263–12273. https://doi.org/10.1029/2018GL080613

Klein, E., Métois, M., Meneses, G., Vigny, C., & Delorme, A. (2018). Bridging the gap between North and Central Chile: Insight from new GPS data on coupling complexities and the Andean sliver motion. *Geophysical Journal International*, *213*(3), 1924–1933. https://doi.org/10.1093/gji/ggy094

Klein, E., Potin, B., Pasten-Araya, F., Tissandier, R., Azua, K., Duputel, Z., et al. (2021). Interplay of seismic and a-seismic deformation during the 2020 sequence of Atacama, Chile. *Earth and Planetary Science Letters*, *570*, 117081. https://doi.org/10.1016/j.epsl.2021.117081

Klein, E., Vigny, C., Duputel, Z., Zigone, D., Rivera, L., Ruiz, S., & Potin, B. (2023). Return of the Atacama deep slow slip event: The 5-year recurrence confirmed by continuous GPS. *Physics of the Earth and Planetary Interiors*, *334*, 106970. https://doi.org/10.1016/j.pepi.2022.106970

Köhne, T., Riel, B., & Simons, M. (2023). Decomposition and inference of sources through spatiotemporal analysis of network signals: The DISSTANS python package. *Computers & Geosciences*, *170*, 105247. https://doi.org/10.1016/j.cageo.2022.105247

Lay, T., Kanamori, H., Ammon, C. J., Koper, K. D., Hutko, A. R., Ye, L., et al. (2012). Depth-varying rupture properties of subduction zone megathrust faults. *Journal of Geophysical Research*, *117*(4), B04311. https://doi.org/10.1029/2011JB009133

Li, S., Moreno, M., Bedford, J., Rosenau, M., & Oncken, O. (2015). Revisiting viscoelastic effects on interseismic deformation and locking degree: A case study of the Peru-north Chile subduction zone. *Journal of Geophysical Research: Solid Earth*, *120*(6), 4522–4538. https://doi.org/10.1002/2015JB011903

Métois, M., Vigny, C., & Socquet, A. (2016). Interseismic coupling, megathrust earthquakes and seismic swarms along the Chilean subduction zone (38°–18°S). *Pure and Applied Geophysics*, *173*(5), 1431–1449. https://doi.org/10.1007/s00024-016-1280-5

Molina, D., Tassara, A., Abarca, R., Melnick, D., & Madella, A. (2021). Frictional segmentation of the Chilean megathrust from a multivariate analysis of geophysical, geological, and geodetic data. *Journal of Geophysical Research: Solid Earth*, *126*(6), e2020JB020647. https://doi.org/10.1029/2020JB020647

Moreno, M., Haberland, C., Oncken, O., Rietbrock, A., Angiboust, S., & Heidbach, O. (2014). Locking of the Chile subduction zone controlled by fluid pressure before the 2010 earthquake. *Nature Geoscience*, *7*(4), 292–296. https://doi.org/10.1038/ngeo2102

Moreno, M., Li, S., Melnick, D., Bedford, J., Baez, J. C., Motagh, M., et al. (2018). Chilean megathrust earthquake recurrence linked to frictional contrast at depth. *Nature Geoscience*, *11*(4), 285–290. https://doi.org/10.1038/s41561-018-0089-5

Mousavi, S. M., Ellsworth, W. L., Zhu, W., Chuang, L. Y., & Beroza, G. C. (2020). Earthquake transformer—An attentive deep-learning model for simultaneous earthquake detection and phase picking. *Nature Communications*, *11*(1), 3952. https://doi.org/10.1038/s41467-020-17591-w

Mousavi, S. M., Sheng, Y., Zhu, W., & Beroza, G. C. (2019). STanford EArthquake dataset (STEAD): A global data set of seismic signals for AI. *IEEE Access*, *7*, 179464–179476. https://doi.org/10.1109/access.2019.2947848

Münchmeyer, J., Woollam, J., Rietbrock, A., Tilmann, F., Lange, D., Bornstein, T., et al. (2022). Which picker fits my data? A quantitative evaluation of deep learning based seismic pickers. *Journal of Geophysical Research: Solid Earth*, *127*(1), e2021JB023499. https://doi.org/10.1029/2021JB023499

Obara, K., & Kato, A. (2016). Connecting slow earthquakes to huge earthquakes. *Science*, *353*(6296), 253–257. https://doi.org/10.1126/science.aaf1512

Ohta, Y., Freymueller, J. T., Hreinsdóttir, S., & Suito, H. (2006). A large slow slip event and the depth of the seismogenic zone in the south central Alaska subduction zone. *Earth and Planetary Science Letters*, *247*(1), 108–116. https://doi.org/10.1016/j.epsl.2006.05.013

Ojeda, J., Morales-Yáñez, C., Ducret, G., Ruiz, S., Grandin, R., Doin, M.-P., et al. (2023). Seismic and aseismic slip during the 2006 Copiapo swarm in North-Central Chile. *Journal of South American Earth Sciences*, *123*, 104198. https://doi.org/10.1016/j.jsames.2023.104198

Okamoto, K. K., Savage, H. M., Cochran, E. S., & Keranen, K. M. (2022). Stress heterogeneity as a driver of aseismic slip during the 2011 Prague, Oklahoma aftershock sequence. *Journal of Geophysical Research: Solid Earth*, *127*(8), e2022JB024431. https://doi.org/10.1029/2022JB024431

Ortega-Culaciati, F., Simons, M., Ruiz, J., Rivera, L., & Díaz-Salazar, N. (2021). An epic Tikhonov regularization: Application to quasi-static fault slip inversion. *Journal of Geophysical Research: Solid Earth*, *126*(7), e2020JB021141. https://doi.org/10.1029/2020JB021141

Pastén-Araya, F., Potin, B., Azúa, K., Sáez, M., Aden-Antoniów, F., Ruiz, S., et al. (2022). Along-dip segmentation of the slip behavior and rheology of the Copiapó Ridge subducted in North-Central Chile. *Geophysical Research Letters*, *49*(4), e2021GL095471. https://doi.org/10.1029/2021gl095471

Peng, Z., & Gomberg, J. (2010). An integrated perspective of the continuum between earthquakes and slow-slip phenomena. *Nature Geoscience*, *3*(9), 599–607. https://doi.org/10.1038/ngeo940

Perfettini, H., Avouac, J.-P., Tavera, H., Kositsky, A., Nocquet, J. M., Bondoux, F., et al. (2010). Seismic and aseismic slip on the Central Peru megathrust. *Nature*, *465*(7294), 78–81. https://doi.org/10.1038/nature09062

Poli, P., Jeria, A. M., & Ruiz, S. (2017). The Mw 8.3 Illapel earthquake (Chile): Preseismic and postseismic activity associated with hydrated slab structures. *Geology*, *45*(3), 247–250. https://doi.org/10.1130/G38522.1

Radiguet, M., Perfettini, H., Cotte, N., Gualandi, A., Valette, B., Kostoglodov, V., et al. (2016). Triggering of the 2014 Mw 7.3 Papanoa earthquake by a slow slip event in Guerrero, Mexico. *Nature Geoscience*, *9*(11), 829–833. https://doi.org/10.1038/ngeo2817

Sambridge, M. (2013). A parallel tempering algorithm for probabilistic sampling and multimodal optimization. *Geophysical Journal International*, *196*(1), 357–374. https://doi.org/10.1093/gji/ggt342

Savage, J. C. (1983). A dislocation model of strain accumulation and release at a subduction zone. *Journal of Geophysical Research*, *88*(B6), 4984–4996. https://doi.org/10.1029/JB088iB06p04984

Schurr, B., Moreno, M., Tréhu, A. M., Bedford, J., Kummerow, J., Li, S., & Oncken, O. (2020). Forming a Mogi Doughnut in the years prior to and immediately before the 2014 M8.1 Iquique, northern Chile, earthquake. *Geophysical Research Letters*, *47*(16), e2020GL088351. https://doi.org/10.1029/2020GL088351

Schwartz, S. Y., & Rokosky, J. M. (2007). Slow slip events and seismic tremor at circum-pacific subduction zones. *Reviews of Geophysics*, *45*(3), RG3004. https://doi.org/10.1029/2006RG000208

Sippl, C., Moreno, M., & Benavente, R. (2021). Microseismicity appears to outline highly coupled regions on the Central Chile megathrust. *Journal of Geophysical Research: Solid Earth*, *126*(11), e2021JB022252. https://doi.org/10.1029/2021jb022252

Sippl, C., Schurr, B., Asch, G., & Kummerow, J. (2018). Seismicity structure of the northern Chile forearc from > 100,000 double-difference relocated hypocenters. *Journal of Geophysical Research: Solid Earth*, *123*(5), 4063–4087. https://doi.org/10.1002/2017JB015384

Socquet, A., Baez, J. C., Moreno, M., & Langlais, M., & DEEP-Trigger Team and Geophysics Technical Service at ISTerre and RESIF. (2025). *DEEP-TRIGGER temporary experiment in the subduction zone Peru/Chile, Chile*. RESIF—Réseau Sismologique et géodésique Français. https://doi.org/10.15778/RESIF.XZ2020

Socquet, A., Valdes, J. P., Jara, J., Cotton, F., Walpersdorf, A., Cotte, N., et al. (2017). An 8 month slow slip event triggers progressive nucleation of the 2014 Chile megathrust. *Geophysical Research Letters*, *44*(9), 4046–4053. https://doi.org/10.1002/2017GL073023

Tassara, A., & Echaurren, A. (2012). Anatomy of the Andean subduction zone: Three-dimensional density model upgraded and compared against global-scale models. *Geophysical Journal International*, *189*(1), 161–168. https://doi.org/10.1111/j.1365-246x.2012.05397.x

Teunissen, P. J., & Montenbruck, O. (2017). *Springer handbook of global navigation satellite systems*. Springer International Publishing. https://doi.org/10.1007/978-3-319-42928-1

Thurber, C. H., & Eberhart-Phillips, D. (1999). Local earthquake tomography with flexible gridding. *Computers & Geosciences*, *25*(7), 809–818. https://doi.org/10.1016/S0098-3004(99)00007-2

Tilmann, F., Heit, B., Moreno, M., & González-Vidal, D. (2021). *Anillo*. GFZ Data Services. https://doi.org/10.14470/L17575324477

Tilmann, F., Zhang, Y., Moreno, M., Saul, J., Eckelmann, F., Palo, M., et al. (2016). The 2015 Illapel earthquake, central Chile: A type case for a characteristic earthquake. *Geophysical Research Letters*, *43*(2), 574–583. https://doi.org/10.1002/2015GL066963

Uchida, N., & Bürgmann, R. (2019). Repeating earthquakes. *Annual Review of Earth and Planetary Sciences*, *47*(1), 305–332. https://doi.org/10.1146/annurev-earth-053018-060119

Uchida, N., & Matsuzawa, T. (2013). Pre- and postseismic slow slip surrounding the 2011 Tohoku-oki earthquake rupture. *Earth and Planetary Science Letters*, *374*, 81–91. https://doi.org/10.1016/j.epsl.2013.05.021

Universidad de Chile. (2013). *Red Sismologica Nacional*. International Federation of Digital Seismograph Networks. https://doi.org/10.7914/SN/C1

Vallée, M., Nocquet, J. M., Battaglia, J., Font, Y., Segovia, M., Régnier, M., et al. (2013). Intense interface seismicity triggered by a shallow slow slip event in the Central Ecuador subduction zone. *Journal of Geophysical Research: Solid Earth*, *118*(6), 2965–2981. https://doi.org/10.1002/jgrb.50216

VMF Data Server. (2021). In re3data.org: VMF data server; editing status 2021-08-24; re3data.org—registry of research data repositories. https://doi.org/10.17616/R3RD2H

Voss, N., Dixon, T. H., Liu, Z., Malservisi, R., Protti, M., & Schwartz, S. (2018). Do slow slip events trigger large and great megathrust earthquakes? *Science Advances*, *4*(10), eaat8472. https://doi.org/10.1126/sciadv.aat8472

Waldhauser, F., & Ellsworth, W. L. (2000). A double-difference earthquake location algorithm: Method and application to the northern Hayward Fault, California. *Bulletin of the Seismological Society of America*, *90*(6), 1353–1368. https://doi.org/10.1785/0120000006

Wang, K., & Bilek, S. L. (2014). Invited review paper: Fault creep caused by subduction of rough seafloor relief. *Tectonophysics*, *610*, 1–24. https://doi.org/10.1016/j.tecto.2013.11.024

Woollam, J., Münchmeyer, J., Tilmann, F., Rietbrock, A., Lange, D., Bornstein, T., et al. (2022). SeisBench—A toolbox for machine learning in seismology. *Seismological Research Letters*, *93*(3), 1695–1709. https://doi.org/10.1785/0220210324

Yáñez-Cuadra, V., Ortega-Culaciati, F., Moreno, M., Tassara, A., Krumm-Nualart, N., Ruiz, J., et al. (2022). Interplate coupling and seismic potential in the Atacama seismic gap (Chile): Dismissing a rigid Andean sliver. *Geophysical Research Letters*, *49*(11), 1–26. https://doi.org/10.1029/2022gl098257

Zhan, Z. (2020). Mechanisms and implications of deep earthquakes. *Annual Review of Earth and Planetary Sciences*, *48*(1), 147–174. https://doi.org/10.1146/annurev-earth-053018-060314

Zhu, W., McBrearty, I. W., Mousavi, S. M., Ellsworth, W. L., & Beroza, G. C. (2022). Earthquake phase association using a Bayesian Gaussian mixture model. *Journal of Geophysical Research: Solid Earth*, *127*(5), e2021JB023249. https://doi.org/10.1029/2021JB023249